NUMERICAL STUDY ON MODELING OF LIQUID FILM FLOW UNDER COUNTERCURRENT FLOW LIMITATION IN VOLUME OF FLUID METHOD

T. Watanabe and T. Takata
Department of Sustainable Energy and Environmental Engineering
Osaka University
2-1 Yamadaoka, Suita-shi, Osaka, 565-0871, Japan
watanabe_t@qe.see.eng.osaka-u.ac.jp; takata_t@see.eng.osaka-u.ac.jp

A. Yamaguchi
The University of Tokyo
7-3-1 Hongo, Bunkyo-ku, Tokyo, 113-0033, Japan
yamaguchi@n.t.u-tokyo.ac.jp

ABSTRACT

Countercurrent flow Limitation (CCFL) in a heat transfer tube at the SG has an influence on the core cooling under a loss of coolant accident (LOCA) in a pressurized water reactor (PWR) because no liquid flows downstream after the CCFL. In order to improve the prediction accuracy of the CCFL characteristic in numerical simulations using the volume of fluid (VOF) method, a thin liquid film flow in a countercurrent flow is modeled separately from the VOF simulation and is coupled with VOF method. The CCFL characteristic was estimated analytically using the condition of maximizing quantity of a liquid film with respect to a void fraction or a liquid film thickness. Additionally, we have modified the estimated CCFL characteristic with the critical thickness of liquid film as criteria of a liquid film thickness. Then, we have proposed the coupling method with VOF simulation by using the flow network of virtual liquid film based on the transport of water by thin liquid film flow and have carried out numerical simulations of a countercurrent flow in a vertical tube. Furthermore, it was concluded that the experimental and numerical uncertainty of the CCFL characteristics will caused by the flow structure near the tube end and the upward flux.

KEYWORDS
Liquid film flow, CCFL, VOF method, Countercurrent annular flow, PWR

1. INTRODUCTION

A heat removal by reflux condensation of vapor at a steam generator (SG) is considered as one of the possible core cooling methods under a loss of coolant accident (LOCA) in a pressurized water reactor (PWR). In the reflux condensation, a countercurrent flow is formed in a vertical section of heat transfer tube at the SG. In the heat transfer tube, the vapor generated in the core flows upward in the center, whereas condensed water flows downward along the peripheral. When the velocity of the vapor phase increases, it prevents the water from an outflow through the tube. This process is designated as a countercurrent flow limitation (CCFL). The CCFL affects the cooling performance in the reactor, therefore it is important to estimate the CCFL characteristic. In particular, the CCFL condition in which

falling water flow rate becomes zero, or no liquid film flowing downstream, is quite important because of the criteria of operating limit of reflux condensation by the SG.

A disturbed gas-liquid interface under CCLF is called flooding. There has been considerable research to understand the flooding by air-water experiments and by theoretical analysis [1] [2] [3]. In addition, numerical simulations for the CCFL have been carried out. Generally, CCFL characteristic, which is relationship between a gas and a liquid flow rates in the flooding condition, is expressed by using the Wallis correlation or Wallis parameters [1] which are respectively defined as follows:

$$\sqrt{J_G{}^*} + m\sqrt{J_G{}^*} = C \tag{1}$$

$$J_k{}^* = J_k \sqrt{\frac{\rho_k}{g \cdot D(\rho_L - \rho_G)}}, \quad (k = G, L) \tag{2}$$

where J [m/s] is the volumetric flux, J^* is non-dimensional volumetric flux, m and C are empirical constants, D [m] is the diameter of a vertical tube, g [m/s^2] is the gravity acceleration, and ρ [kg/m^3] is the density. The subscripts L and G denote the gas and liquid phases respectively.

A volume of fluid (VOF) method is mostly used in an industrial field to investigate two-phase flow numerically. However, there are various scales of liquid film flow in CCFL condition therefore it takes much computational cost to simulate CCFL condition with thin liquid film flow in a numerical simulation directly. In this study, a thin liquid film flow in a countercurrent flow is modeled separately from the VOF simulation and is coupled with VOF method in order to improve the prediction accuracy of the CCFL characteristic with less computational cost. At first, we have analytically estimated the CCFL characteristic by using the one-dimensional liquid film flow model. Then, we have proposed the coupling method with VOF simulation by using the flow network of virtual liquid film based on the transport of water by thin liquid film flow, have carried out numerical simulations of a countercurrent flow in a vertical tube and have discussed our present method.

2. LIQUID FILM FLOW MODEL UNDER COUNTERCURRENT FLOW

In this chapter, we assume that an air-water countercurrent flow in a vertical tube is an annular flow. The one-dimensional governing equations under the steady state flow are derived from the momentum balance at the cylindrical coordinate. In the previous study [4], we have investigated an annular flow model based on boundary layer equations or balk velocities. As a result of the comparison with experiment data [5], the model based on balk velocities is good for the estimation of CCFL characteristic. Thus, in this paper, the model based on balk velocities is used.

2.1 Governing Equations

Figure 1 shows the countercurrent annular flow under the steady state in a vertical pipe. In this model, the velocity profiles of gas and liquid phases are not considered. Instead, the balk velocities of gas and liquid phases, u_G and u_L, are used. This one-dimensional model is proposed by Sudo [6] and Monde [7]. δ is a liquid film thickness. τ_i and τ_w are the interface and wall shear stresses. Even though the liquid film thickness varies under the flooding, the time averaged δ and velocity of a liquid film, u_L, can be thought constant when gas flow rate is constant in the steady state flow.

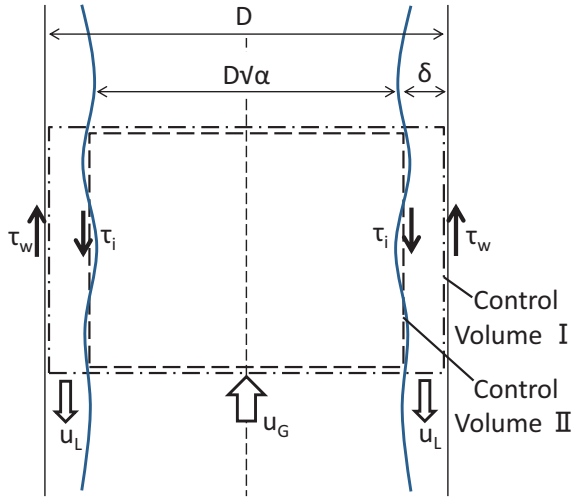

Figure 1. Momentum balance of countercurrent annular flow

Control volume I consists of overall flow in a cross-section, and Control volume II consists of only a gas phase. Here, α is the void fraction and written as $\alpha = (1-2\delta/D)^2$. The momentum balance of Control volume I is:

$$-\frac{\partial p}{\partial z}\frac{\pi D^2}{4} + \tau_W \pi D - [\rho_G \alpha + \rho_L(1-\alpha)]g\frac{\pi D^2}{4} = 0 \tag{3}$$

Then, the momentum balance of Control volume II is:

$$-\frac{\partial p}{\partial z}\frac{\pi D^2}{4}\alpha - \tau_i \pi D\sqrt{\alpha} - \rho_G \alpha g\frac{\pi D^2}{4} = 0 \tag{4}$$

By deleting *dp/dz* in Eq. (3) and Eq. (4), the governing equation is given as follows:

$$\frac{4\tau_i}{D\sqrt{\alpha}} + \frac{4\tau_w}{D} - (\rho_L - \rho_G)(1-\alpha)g = 0 \tag{5}$$

where, the interface shear stress τ_i and the wall shear stress τ_w based on relative velocities at interface are given as follows:

$$\tau_i = \frac{1}{2}f_i\rho_G(u_G + u_L)^2 = \frac{1}{2}f_i\rho_G\left[\frac{J_G}{\alpha} + \frac{J_L}{(1-\alpha)}\right]^2 \tag{6}$$

$$\tau_w = \frac{1}{2}f_w\rho_L {u_L}^2 = \frac{1}{2}f_w\rho_L\frac{{J_L}^2}{(1-\alpha)^2} \tag{7}$$

where f_i is the interfacial friction coefficient and f_w is the wall friction coefficient. By using Eq. (2), Eq. (6) and Eq. (7), Eq. (5) is transformed into:

$$\frac{2f_i}{\alpha^{5/2}}\left[J_G^* + \frac{\alpha}{(1-\alpha)}\left(\frac{\rho_G}{\rho_L}\right)^{1/2}J_L^*\right]^2 + \frac{2f_w}{(1-\alpha)^2}J_L^{*2} - (1-\alpha) = 0 \tag{8}$$

Here, the number of unknown variables is five, or, J_G, J_L, α, f_i and f_w in Eq. (8). Therefore, the other four constitutive equations are required in order to solve Eq. (8).

2.2 Constitutive Equations of CCFL

2.2.1 Maximum quantity of a liquid film

The countercurrent flow model explained in Section 2.1 has infinite flow patterns, because the number of unknown variables is larger than that of independent equations. In the estimation of CCFL characteristic, it is important to estimate the value of J_L under the condition of given J_G. If J_G is given, the number of necessary constitutive equations is three in Eq. (8). In this study we assign empirical correlations to the coefficients, f_i and f_w, in Eq. (8) therefore the number of necessary constitutive equations is also one in Eq. (8).

Sudo [6] reported that when J_G is constant, the CCFL condition is given by the condition that a liquid volumetric flux, J_L, becomes the maximum value with respect to a void fraction or a liquid film thickness as follows:

$$\frac{\partial J_L}{\partial \alpha} = 0, \ or \ \ \frac{\partial J_L}{\partial \delta} = 0 \tag{9}$$

This condition is derived from an envelope proposed by Bharathan et al. [3]. He reported that an envelope of governing equation of a countercurrent flow gives the condition of initiate flooding.

2.2.2 Interfacial and wall friction coefficients

Eq. (8) contains the interfacial friction coefficient, f_i, and the wall friction coefficient, f_w, as unknown variables. Here, f_i and f_w are given by the following equations proposed by Sudo [6]:

$$\begin{aligned} f_i &= 0.008\left\{1 + m \cdot \left(\frac{\delta}{D}\right)^n\right\} \\ n &= 1.63 + 4.74/Bo \\ m &= 41.3 \cdot Bo^{(n+0.25)} \cdot 10^{\frac{9.07}{Bo}} \\ Bo &= \{(\rho_L - \rho_G) \cdot g/\sigma\}^{1/2} \cdot D \end{aligned} \tag{10}$$

$$\begin{aligned} f_w &= A \cdot {Re_L}^B \\ Re_L < 2000 \ \ (\text{laminar}) &: A = 16.0, \ B = -1.0 \\ 2000 \le Re_L < 4000 \ \ (\text{transition}) &: A = 1.76 \times 10^{-10}, \ B = 2.32 \\ Re_L \ge 4000 \ \ (\text{turbulent}) &: A = 0.314, \ B = -0.25 \end{aligned} \tag{11}$$

where σ is the surface tension. Bo is non-dimensional number. By adapting Eq. (9), Eq. (10) and Eq.(11) to Eq. (8), the number of necessary constitutive equations is satisfied.

2.2.3 Critical thickness of liquid film

A liquid film thickness, δ, is a function of a void fraction. The calculated liquid film thickness is able to be infinitely small. However, real liquid film is thought to vanish when a liquid film thickness is less than a limit. Therefore we introduce "critical thickness of liquid film, δ_{min}," as criteria of a liquid film thickness which are proposed by Ito et al. [8] as follows:

$$\delta_{min} = 4.54 \cdot \left(\frac{g}{{\nu_L}^2}\right)^{-1/3} \quad (12)$$

where ν_L is the dynamic viscosity of liquid. If a calculated liquid film thickness is less than the critical thickness of liquid film ($\delta < \delta_{min}$), we assume that δ and J_L equal to zero because there may be no liquid film in physical process.

2.3 Analytical Results and Discussions

Figure 2 shows the estimated CCFL characteristic, which is relationship between ${J_G}^{*1/2}$ and ${J_L}^{*1/2}$, compered experiment data [5] [9]. In this study, gas and liquid flow rates (volumetric fluxes: J_G and J_L) are arranged by the Wallis parameters expressed by Eq. (2). The experimental CCFL characteristics are different between D = 0.019 m and D = 0.02 m even in almost the same diameter. Figure 3 shows the schematics of experimental apparatus [5] [9], respectively. In the experiment [9] (D = 0.02m), CCFL occurred at the lower end of the pipe. Since it is found that the characteristic strongly depends on the flooding locations (upper end, lower end and inside pipe) which are different due to shapes at the upper and lower end by Jeong et al. [10], it is though that CCFL occurred at the upper end or inside pipe in the experiment [5] (D = 0.019m).

Overall, the model based on balk velocities (original) agrees with experiment data [5] because Eq. (8) expresses the momentum balance of the inside pipe. However, the original model doesn't agree with experiment data [5] in ${J_G}^{*1/2} < 0.4$ at D = 0.019 m. The modified line overlap with the original one in the region of ${J_G}^{*1/2} < 0.8$ at D = 0.019 m and ${J_G}^{*1/2} < 0.75$ at D = 0.064 m. The gradient of the line changes in the point where the wall friction coefficient, f_w, shifts. The calculated liquid film thickness becomes smaller with the increasing gas flow rate and is less than the critical thickness of liquid film in the region of when ${J_G}^{*1/2} > 0.8$ at D = 0.019 m and ${J_G}^{*1/2} > 0.7$ at D = 0.064 m. In these region, ${J_L}^{*1/2}$ is modified to ${J_L}^{*1/2} = 0$. In $0.8 < {J_G}^{*1/2} < 0.9$ at D = 0.019 m and in $0.7 < {J_G}^{*1/2} < 0.72$ at D = 0.064 m, ${J_L}^{*1/2}$ of the original model is modified. The modified range of ${J_G}^{*1/2}$ is large when the diameter is small.

In addition to save a computational cost, so as to investigate the difference between experiments [5] [9], the liquid film flow model is coupled with a numerical simulation.

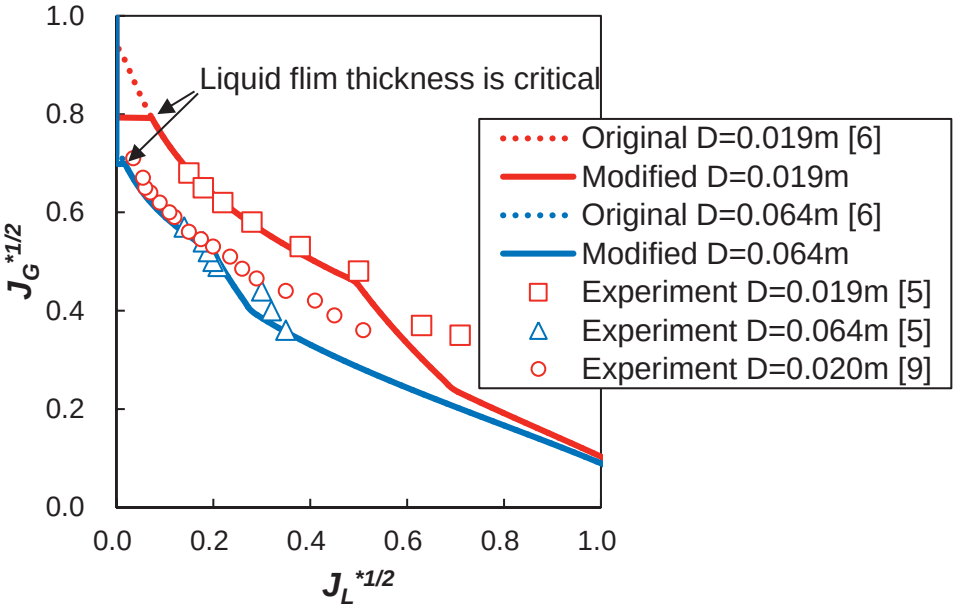

Figure 2. Estimated CCFL characteristic and liquid film thickness

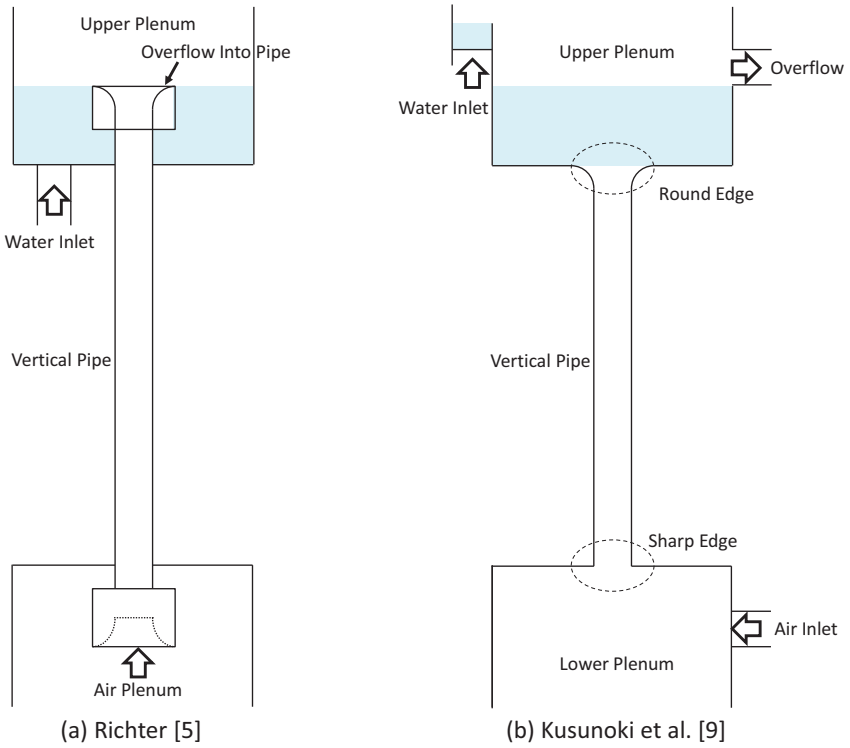

Figure 3. Schematics of experimental apparatus

3. COUPLING WITH VOF METHOD

3.1 Flow Network of Virtual Liquid Film

In this study, thin liquid film flow is model separately from the two-dimensional VOF simulation. In this thin liquid film flow model, the virtual computational region is configured for the liquid film out of numerical resolution of VOF simulation. In the virtual computational region, liquid phase flows downward and is transported independently of VOF method. The transported liquid mass is based on mass conservation and calculated by the one-dimensional liquid film flow model explained in Chapter 2.

3.1.1 Governing equations

Figure 4 shows the schematic of thin liquid film flow in VOF simulation. We assume that the thin liquid film virtually flows downward along the vertical tube surface under the steady state. The virtual liquid film flows from above to below only in vertical tube and doesn't flows in an opposite direction. Then, the mass conservation of liquid for a control volume in a vertical direction is given by following equation:

$$G_{in} - G_{out} - G_{VOF} = 0 \tag{13}$$

where G_{in} [kg/s] and G_{out} [kg/s] are the inflow and the outflow rate of masses through the control volume respectively. G_{VOF} [kg/s] is the exchange mass flow rate with VOF simulation.

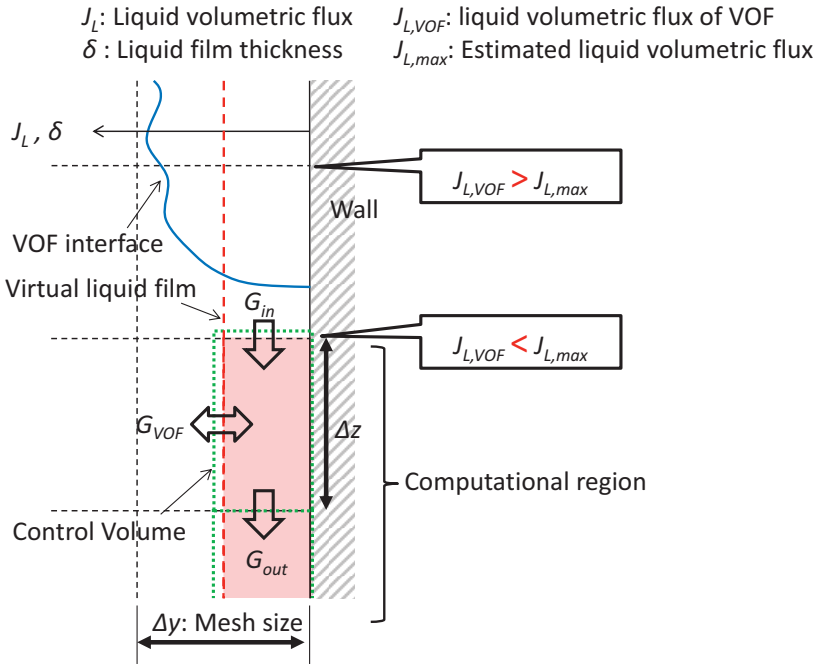

Figure 4. Schematic of flow network of virtual liquid film

The virtual liquid film is coupled with VOF simulation through G_{VOF} in Eq. (13). G_{VOF} is converted to a VOF function and is added to the transport equation of VOF function and the continuity equation in VOF method as a source term. The transport equation of VOF function is as follows:

$$\frac{\partial f}{\partial t} + \boldsymbol{u} \cdot \nabla f = S_f \tag{14}$$

The continuity equation is as follows:

$$\nabla \cdot \boldsymbol{u} = S_f \tag{15}$$

where f [-] is the VOF function, S_f [1/s] is the source term of VOF function.

3.1.2 Numerical procedure

The flow network of virtual liquid film shown in Fig. 4 is half side in the tube. The other side is similar to Fig. 4. The numerical procedure for the flow network of virtual liquid film is as follows:

(I) Calculation of values at each cross-section
At a time step, the gas and liquid volumetric fluxes at each cross-section of the tube ($J_{G,VOF}$ and $J_{L,VOF}$) is calculated from VOF simulation values. Using $J_{G,VOF}$ as a input value, the estimated liquid volumetric flux, $J_{L,max}$, and the estimated liquid film thickness, δ_{max}, are calculated from Eq. (8) and Eq. (9).

(II) Configuration of computational region
The computational region of virtual liquid film satisfies following conditions at a cross-section: (1) the estimated liquid film thickness is less than mesh size of a wall adjacent cell ($\delta_{max} < \Delta y$). That is, the estimated liquid film thickness is out of numerical resolution. (2) The estimated liquid film thickness is larger than the critical thickness of liquid film ($\delta_{max} > \delta_{min}$). And (3) the estimated liquid volumetric flux is larger than the liquid volumetric flux of VOF simulation ($J_{L,max} > J_{L,VOF}$). The conditions of (1) and (3) are based on the concept that we depend on VOF method in thick liquid film and large falling water rate.

(III) Inlet boundary
The liquid is extracted from a cell of VOF simulation, which locates on upper side of the inlet control volume of virtual liquid film, to virtual liquid film. The inflow rate of mass, G_{in}, is evaluated by the estimated liquid volumetric flux, $J_{L,max}$, which is converted to a mass flow rate at inlet cross-section. However, the inflow rate of mass is limited so as not to exceed liquid mass of the simulation in the extracted cell

(IV) Calculation of control volumes in computational region
G_{in} and G_{out} in Eq. (13) are evaluated by the estimated liquid volumetric flux, $J_{L,max}$, which is converted to a mass flow rate at a cross-section. G_{in} equals to G_{out} of the upper control volume. G_{VOF} is the difference between G_{in} and G_{out}. When G_{VOF} is positive, liquid is added to VOF simulation. When G_{VOF} is negative, liquid is extracted from VOF simulation. G_{VOF} is coupled with VOF simulation at a wall adjacent cell. Considering a flow direction, the outflow rate of mass, G_{out}, is limited so as not to exceed the total mass of the inflow mass and the exchange mass with VOF simulation ($G_{out} \leq G_{in} - G_{VOF}$).

(V) Outlet boundary
The liquid which outflows through lower end of virtual liquid film is added to a cell of VOF simulation which locates on lower side of the outlet control volume of virtual liquid film.

3.1.3 Applicable range of virtual liquid film

Figure 5 shows the relationship between the estimated CCFL characteristic or liquid film thickness explained in Chapter 2 and the flow network of virtual liquid film. The ranges satisfied following conditions with respect to J_G are "not" computational region of virtual liquid film. (1) The estimated

liquid film thickness is larger than mesh size of a wall adjacent cell ($\delta_{max} > \Delta y$). (2) The estimated liquid film thickness is less than the critical thickness of liquid film ($\delta_{max} < \delta_{min}$). (3) The estimated liquid volumetric flux is less than the liquid volumetric flux of VOF simulation ($J_{L,max} < J_{L,VOF}$) although out of region (1) and (2). However, $J_{L,VOF}$ is calculated from a volumetric flux in a wall adjacent cell only so as to ignore the effect of droplets and back-flow. Consequently, the computational region of virtual liquid film is white area as shown in Fig. 5.

Let us discuss a sensitivity of the critical thickness. Table I shows the result at D = 0.02 m. When the critical thickness varies in $\pm$10 %, the Wallis parameter ($J_G^{*1/2}$) changes from - 3.4 % to + 3.0 %. Accordingly, it can be said that the critical thickness has a comparative low influence on the Wallis parameters.

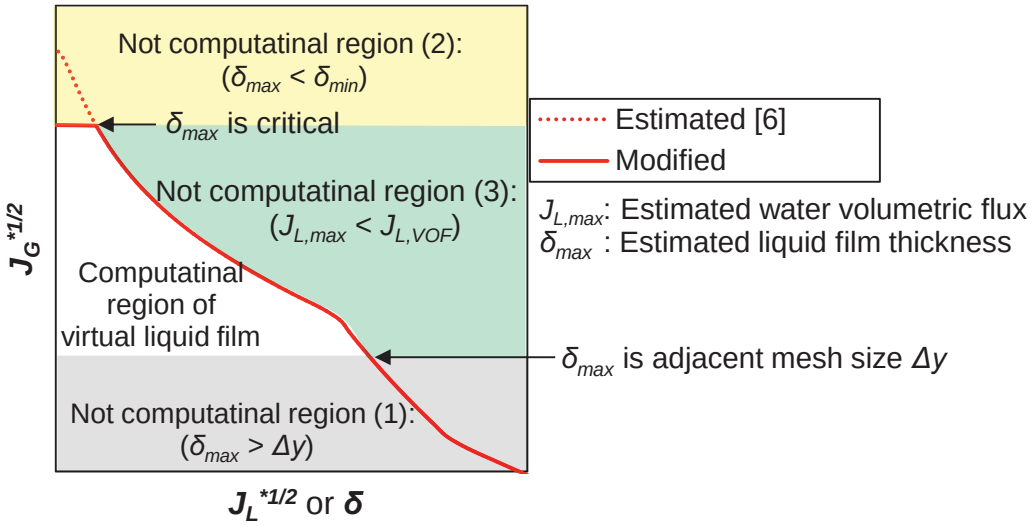

Figure 5. Applicable range of virtual liquid film

Table I. Sensitivity for the critical thickness of liquid film; D = 0.02 m

Rate of critical film thickness change	**-10 %**	**0 %**	**+10%**
Critical film thickness: δ_{min} [m]	1.91×10^{-4}	2.13×10^{-4}	2.34×10^{-4}
Non-dimensional gas volumetric flux at $\delta_{max} = \delta_{min}$: $J_G^{*1/2}$ [-]	0.819 (+3.0 %)	0.795	0.768 (-3.4 %)

3.2 Analytical Conditions

A two-dimensional numerical simulation of air-water countercurrent flow is carried out by using the VOF method. The in-house numerical analysis code with VOF method was used. As a numerical solution, the code uses PLIC [11] (Piecewise Linear Interface Calculation) to consider the interfacial gradient, the CSF (Continuum Surface Force) model [12] to calculate a surface tension, and SMAC (Simplified Maker and Cell) method.

Figure 6 shows the analytical model for which a finite difference with a structural mesh arrangement in Cartesian coordinates is applied. The inner diameter D of the tube was 0.02 m, which corresponds to the

diameter of U-tubes in an actual SG. The tube length L was 0.5 m. In the previous experiment [9], the CCFL characteristic doesn't be affected by L when the L is over 0.3 m. In this benchmark analysis, the mesh was arranged roughly. The wall adjacent cells of the tube were 1.0×10^{-3} m in a horizontal direction, which is one order of magnitude larger than the critical thickness of liquid film (around 2.0×10^{-4} m). In a vertical direction, the cells were 1.0×10^{-2} m. The VOF code used fractional time step for SMAC method and the transport equation of VOF function, respectively. The flow field was laminar. The pressure was 0.1 MPa. The temperature was 20°C. The surface tension σ was 0.0728 N/m. The contact angle was 45°. The boundary condition of constant pressure was used at the outlet. The air was injected to lower tank by the constant velocity boundary. The water was injected from the wall of the tube by the constant velocity boundary in order to prevent CCFL at upper end of the tube and to simulate water condensation in the SG. The other boundaries were non-slip condition. The falling water rate was calculated by integrating water volumetric flux which passes through lower end of the tube. The upward and the downward water volumetric fluxes were calculated separately. The total falling water rate was calculated by subtracting the upward water volumetric flux from the downward one.

In this analysis, the injected water volumetric flux was constant at $J_{L,in}$ = 0.11 m/s ($J_{L,in}^{*1/2}$ = 0.5). Under constant injected water, we gradually increased the injected gas volumetric flux.

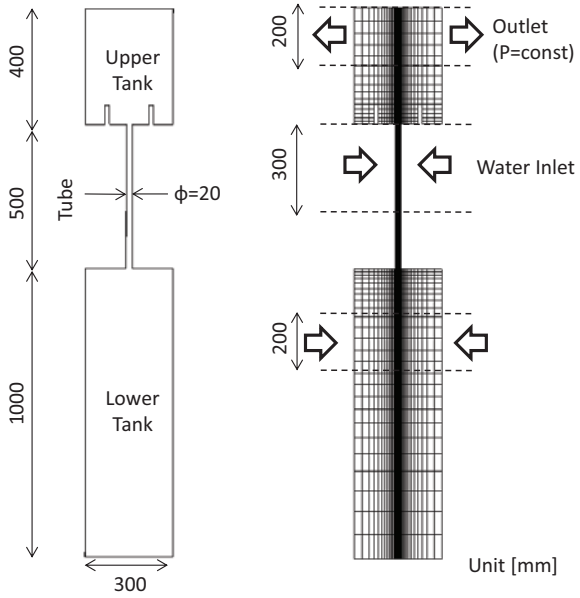

Figure 6. Analytical model and mesh arrangement

3.3 Results and Discussions

Figures 7 and 8 show the comparison of the CCFL characteristics between experiments and computations and the flow pattern in the analyses, respectively. It is noted that there is no difference in theoretical analysis (the line in Fig. 7) between D = 0.019 m and D = 0.02 m. As shown in Fig. 7, the CCFL characteristic is overestimated (the liquid flow rate toward the lower tank is underestimated) in the present model in case of $J_G^{*1/2} < 0.5$. On the other hand, the prediction of the CCFL characteristic is improved by the present model when $J_G^{*1/2} > 0.6$. It is also found that one experiment [5] almost follows the analytical model (green line in Fig. 7) and both numerical analyses agree with another experiment [9] although the same diameter of the pipe is used in the experiments.

As shown in Fig. 8, a liquid film and a comparative large liquid block exists in the pipe when the gas volumetric flux is comparative low ($J_G^{*1/2}$ = 0.5), whereas only liquid film is investigated in high gas flux ($J_G^{*1/2}$ = 0.8). There is no significant difference between the original and the present models as in Fig. 8.

As shown in Fig. 7, the CCFL characteristic is overestimated even the virtual liquid film model. Therefore, the volumetric flux of flow is segmented into an upward flux and a downward flux at the end of tube. Figure 9 shows the result of the upward and downward fluxes in the computations. In the original model, the downward flux agrees with the theoretical model when $J_G^{*1/2} < 0.6$. In this study, δ_{max}, which comes from the mesh size adjacent to the wall, corresponds to approximately $J_G^{*1/2}$ = 0.4. It may be said that the VOF with PLIC has some capability to a sub-mesh resolution at a certain range. However, when $J_G^{*1/2}$ becomes high ($J_G^{*1/2}$ >0.7), the original model cannot reproduce the downward flux as in Fig. 9 (a).

On the other hand, the downward flux follows the theoretical one even in the high $J_G^{*1/2}$ condition in case of the present model as seen in Fig. 9 (b). At the same time, the upward flux is evaluated as almost the same with the downward flux resulting in the similar tendency regardless of the model. Since the liquid flow behavior after the tube end is strongly affected by the geometrical condition of the tube end, the experimental and numerical uncertainty of the CCFL characteristics will caused by the flow structure near the tube end and the upward flux. As a result, the experimental difference might appear regardless of the similar tube size as shown in Figs. 7 and 9.

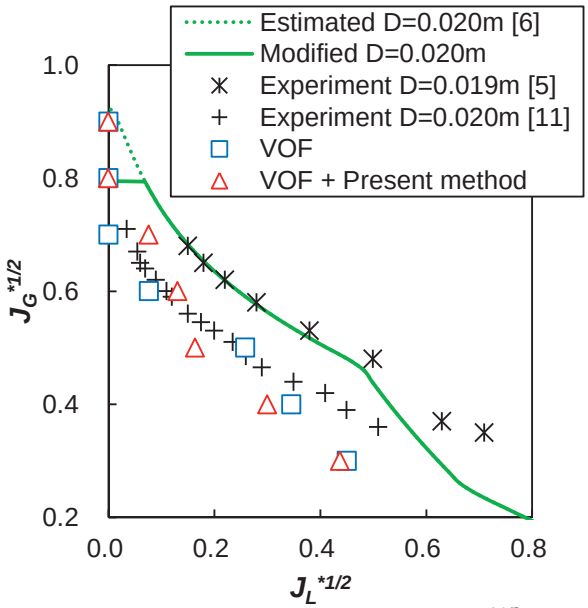

Figure 7. CCFL characteristics in VOF simulation; $J_{L,in}^{*1/2}$ = 0.5 ($J_{L,in}$ = 0.11 m/s)

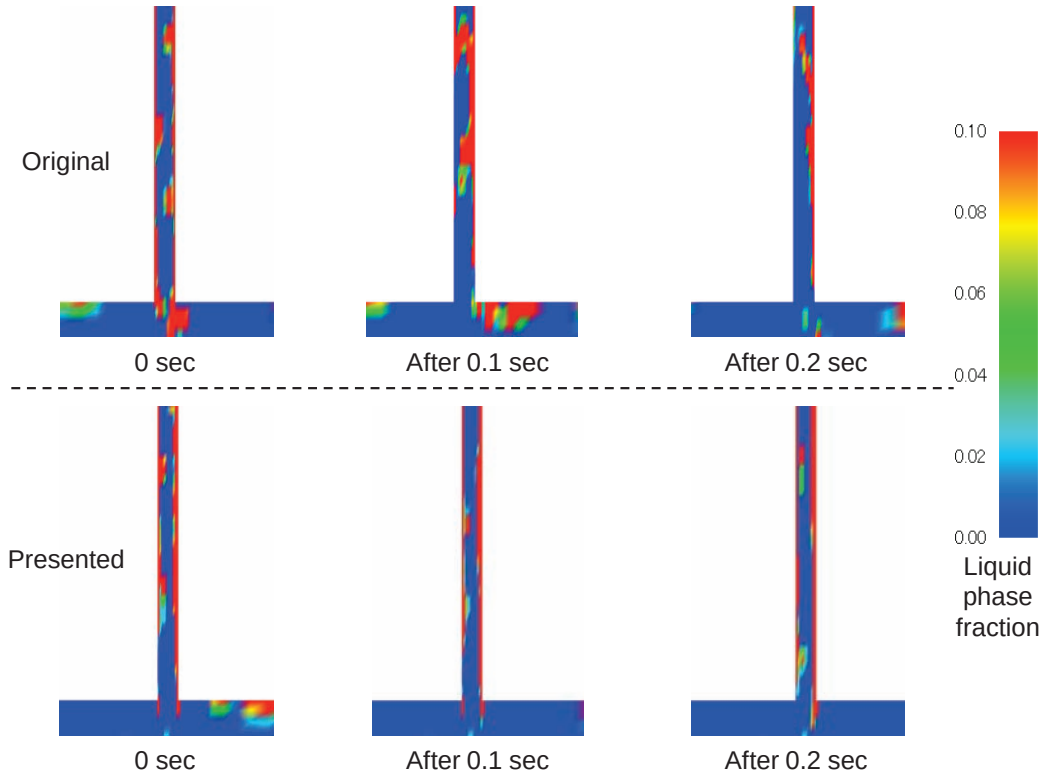

(a) $J_G^{*1/2}$=0.5, $J_{L,in}^{*1/2}$=0.5 (J_G=3.18 m/s, $J_{L,in}$=0.11 m/s)

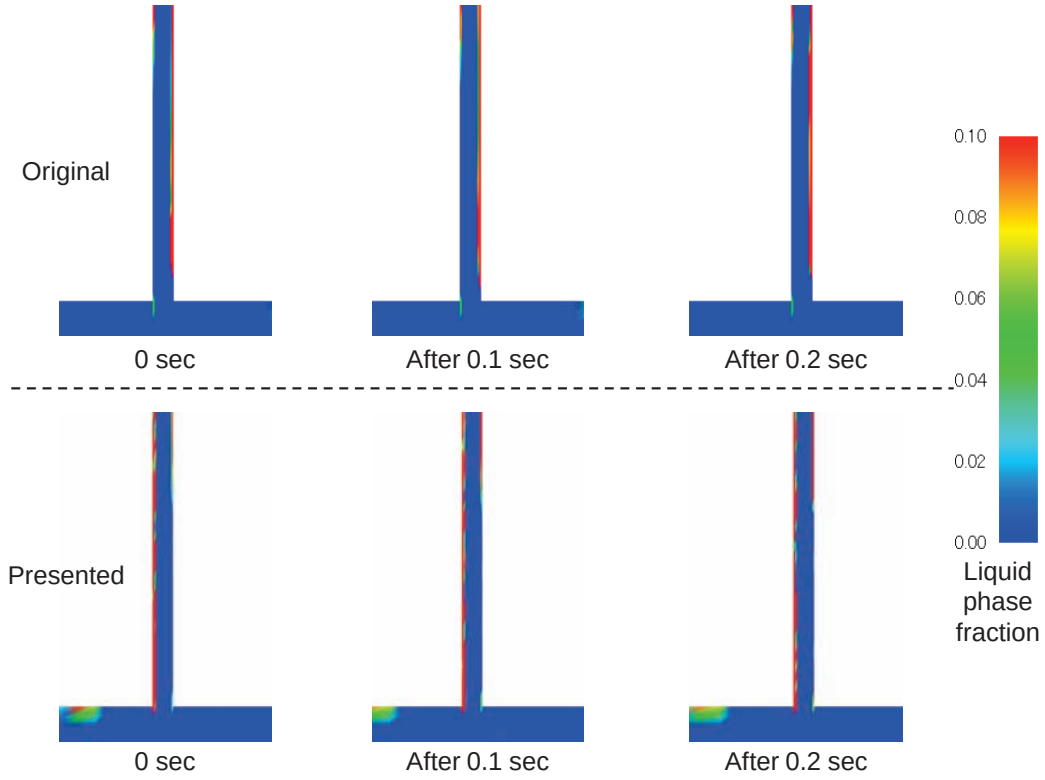

(b) $J_G^{*1/2}$=0.8, $J_{L,in}^{*1/2}$=0.5 (J_G=8.15 m/s, $J_{L,in}$=0.11 m/s)

Figure 8. Flow patterns in VOF simulation; liquid phase fraction range of 0.0-0.1

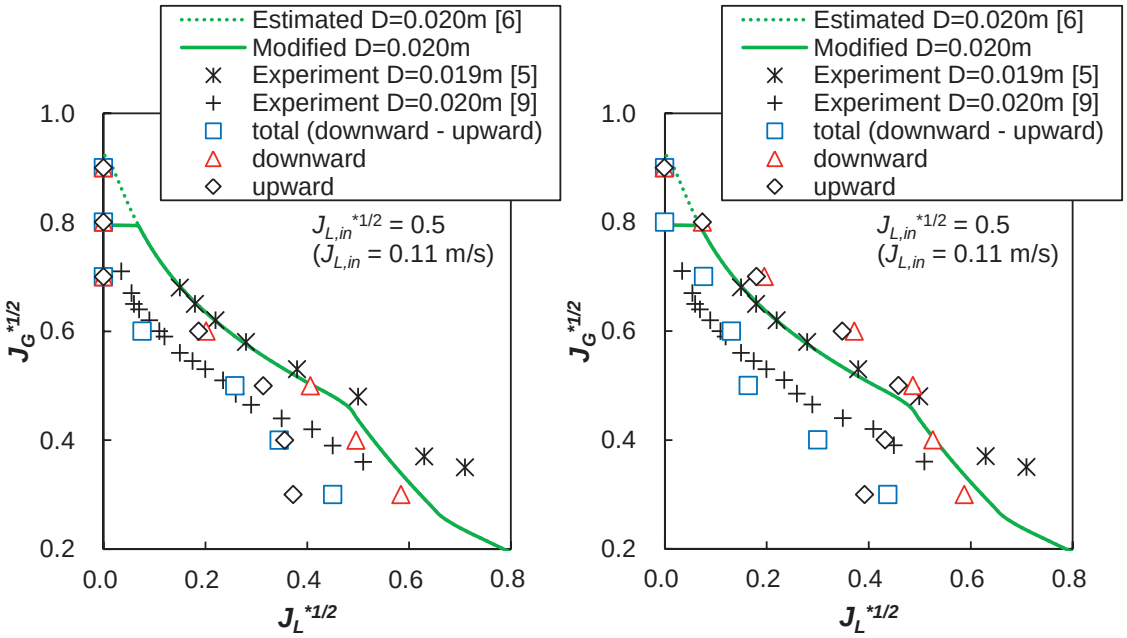

Figure 9. Comparison of downward flow and upward flow at lower end of the tube

4. CONCLUSION

In this study, to improve the prediction accuracy of the CCFL characteristic in a numerical simulation based on VOF method with less computational cost, at first, we have analytically estimated the CCFL characteristic by using the one-dimensional liquid film flow model. The one-dimensional liquid film flow model is based on the momentum balance of air-water countercurrent annular flow with the balk velocities of gas and liquid phases and applies the condition of maximizing quantity of a liquid film with respect to a void fraction or a liquid film thickness. However, the liquid film flow model allows the calculated liquid film thickness to be infinitely small therefore we have introduced the critical thickness of liquid film as criteria of a liquid film thickness and modified the estimated CCFL characteristic.

Next, we have designed the flow network of virtual liquid film and coupled it with VOF method. The flow network of virtual liquid film has the function to transport water by thin liquid film flow in CCFL simulation. The virtual liquid film is based on the mass conservation of liquid film. Its physical quantity is evaluated by the one-dimensional liquid film flow model. The computational region of the flow network of virtual liquid is configured in the region out of numerical resolution of VOF simulation. Then, we have carried out two-dimensional numerical simulations of a countercurrent flow in a vertical tube. As a result of the benchmark analyses, the prediction of the CCFL characteristic was improved by the present model when in the high $J_G^{*1/2}$ condition ($J_G^{*1/2} > 0.6$). Furthermore, it was concluded that the experimental and numerical uncertainty of the CCFL characteristics will caused by the flow structure near the tube end and the upward flux.

NOMENCLATURE

J	volumetric flux	[m/s]
J^*	non-dimensional volumetric flux	[-]
D	diameter	[m]
p	pressure	[Pa]

f_k	friction coefficient	[-]
Re	Reynolds number	[-]
A	constant	[-]
B	constant	[-]
B_o	constant	[-]
n	constant	[-]
m	constant	[-]
f	VOF function	[-]
G	mass flow rate	[kg/m/s]
S_f	source term of VOF function	[1/s]

Greek Letters

ρ	density	[kg/m^3]
δ	liquid film thickness	[m]
v	dynamic viscosity	[m^2/s]
τ	shear stress	[Pa]
α	void fraction	[-]
σ	surface tension	[N/m]

Subscripts

G	gas phase
L	liquid phase
i	interface
w	wall

REFERENCES

1. G. B. Wallis, *One-dimensional Two-phase Flow*, pp. 320-339, McGraw Hill, (1969).
2. H. J. Richter, "Flooding in Tubes and Annuli," *Int. J. Multiphase Flow*, **7**(6), pp. 647-658 (1981).
3. D. Bharathan and G. B. Wallis, "Air-Water Countercurrent Annular Flow," *Int. J. Multiphase Flow*, **9**(4), pp. 349-366 (1983).
4. T. Watanabe, T. Takata and A. Yamaguchi, "Numerical Study on CCFL Condition Based on Thin Film Flow Model Coupled With VOF Method," *The 9th Korea-Japan Symposium on Nuclear Thermal Hy draulics and Safety (NTHAS9)*, Buyeo, Korea, November 16- 19, 2014, N9P0043 (2014).
5. H. J. Richter, "Flooding in Tubes and Annuli," *Int. J. Multiphase Flow*, **7**(6), pp. 647-658 (1981).
6. Y. Sudo, "Analytical Study of Critical Heat Flux under Countercurrent Flow Limitation in Vertical Channels," *Transactions of the JSME Ser. B*, **60**(580), pp. 4222-4228 (1994).
7. M. Monde, "Analysis of Critical Heat Flux in Two-Phase Thermosyphon (Relationship between Maximum Falling Liquid Rate and Critical Heat Flux)," *Transactions of the JSME Ser. B*, **61**(591), pp. 4101-4108 (1995).
8. A. Ito and M. Sasaki, "Breakdown and Formation of a Liquid Film Flowing down an Inclined Plane (1st Report, Measurement of Contact Angle and Mechanism of Film Formation)," *Transactions of the JSME Ser. B*, **52**(475), pp. 1261-1265 (1986).
9. T. Kusunoki, T. Doi, Y. Fujii, T. Tsuji, M. Murase and A. Tomiyama, "Air-Water Tests on Counter-current Flow Limitation at Lower End of Vertical Pipes Simulating Lower Parts of Steam Generator U-tube," *Int. J. Multiphase Flow*, **22**(3), pp. 499-514 (1996).
10. J. H. Jeong and H. C. No, "Experimental Study of the Effect of Pipe Length and Pipe-End Geometry on Flooding," *Journal of J. Multiphase Flow*, **28**(1), pp. 62-70 (2014).
11. W. J. Rider and D. B. Kothe, "Reconstructing Volume Tracking," *Journal of computational physics*, **141**, pp. 112-152 (1998).
12. J. U. Brackbill, D. B. Kothe and C. Zemach, "A Continuum Method for modeling Surface Tension," *Journal of computational physics*, **100**, pp. 335-354 (1992).